Locating Functionalized Gold Nanoparticles Using Electrical Impedance Tomography

Richard H. Bayford, *Life Senior Member, IEEE*, Rui Damaso, Nazanin Neshatvar, *Member, IEEE*, Yevhen Ivanenko, Thomas W Rademacher, Yu Wu, *Member, IEEE*, Nima Seifnaraghi, Lucy Ghali, Nakul Patel, Ivan Roitt, Sven Nordebo, and Andreas Demosthenous *Fellow, IEEE*

Abstract*— *Objective: **An imaging device to locate functionalised nanoparticles, whereby therapeutic agents are transported from the site of administration specifically to diseased tissues, remains a challenge for pharmaceutical research. Here, we show a new method based on electrical impedance tomography (EIT) to provide images of the location of gold nanoparticles (GNPs) and the excitation of GNPs with radio frequencies (RF) to change impedance permitting an estimation of their location in cell models** ***Methods:*** **We have created an imaging system using quantum cluster GNPs as contrast agent, activated with RF fields to heat the functionalized GNPs, which causes a change in impedance in the surrounding region. This change is then identified with EIT.** ***Results:*** **Images of impedance changes of around 80±4% are obtained for a sample of citrate stabilized GNPs in a solution of phosphate-buffered saline. A second quantification was carried out using colorectal cancer cells incubated with culture media, and the internalization of GNPs into the colorectal cancer cells was undertaken to compare them with the EIT images. When the cells were incubated with functionalised GNPs, the change was more apparent, approximately 40±2%. This change was reflected in the EIT image as the cell area was more clearly identifiable from the rest of the area.** ***Significance:*** **EIT can be used as a new method to locate functionalized GNPs in human cells and help in the development of GNP-based drugs in humans to improve their efficacy in the future.**

***Index Terms*—Colorectal cells, electrical impedance tomography (EIT), gold nanoparticles, impedance change, radio frequencies, targeted drug delivery.**

I. Introduction

TARGETED drug delivery, whereby therapeutic agents are transported from the site of administration specifically to diseased tissues, remains a key issue of pharmaceutical research. Nanomedicine, which employs nanoparticle-mediated drug delivery can be used to overcome this problem in conventional drug delivery [1]. Ultra-small nanoparticles that can permeate vessels and move by convection in tissues and cross tissue barriers can be loaded with drugs and can be retained in in specific diseased tissue locations in the body limiting interaction with healthy tissue. The goal is to localise and prolong, drug delivery to focus drug interaction with the diseased tissue. The advantages of this approach are the reduction in the frequency of the dosages taken by the patient and the obtainment of a uniform effect of the drug, that results in minimisation of drug side effects [1]. Transported drugs from the site of administration specifically to diseased tissues, has yet to be achieved. However, targeted delivery would address some of the present limitations and has significant potential to reduce side effects from chemotherapeutic drugs. The development of advanced drug delivery systems (DDS) using pharmaceutical nanotechnology with the capacity to transport small-molecule drugs to tumours, would provide reduced systemic toxicity and improved treatment outcomes [2]. New tools are required to facilitate customisation of therapy based on the specific needs of individual patients. In the drug delivery paradigm, imaging may be used to identify the target and non-target anatomy or for screening, planning, monitoring, and postprocedural assessment of treatment outcome [3].

At present the following methods can be used to track drugs: mass spectrometry (MS) [4], magnetic resonance imaging (MRI) [2], positron emission tomography (PET) [5] and computer tomography (CT). However, there are many limitations with the usage of nanotechnology with these technologies [6], [7]. MS is not a practical technology for use in humans and requires considerable computer processing to build three-dimensional images of the drug location [8]. Tracking drugs using MS is undertaken with animal experiments requiring large scale computing to provide only one image of the accumulation of the drug. PET uses ionizing radiation and requires many minutes to create its images. This technology cannot be used during surgical intervention. It also needs a contrast agent injected into the body and the range of these that are available for PET are not comprehensive or ideal for creating new drugs [5]. CT can track gold nanoparticles (GNPs) but also uses ionizing radiation which limit its use for locating the GNPs [9]. Another limitation is the size; GNPs with

This work was supported by the Engineering and Physical Sciences Research Council (EPSRC) under grant number EP/R04192X/1. The work of YI and SN was funded by the Swedish Foundation for Strategic Research (SSF), grant number AM13-0011. The work of YI was supported by Erasmus under the Erasmus+ Training Programme.

R. H. Bayford, R. Damaso, N. Seifnaraghi, L. Ghali, N. Patel, I. Roit are with the Department of Natural Sciences, Middlesex University, London, UK. (correspondence e-mail: r.bayford@mdx.ac.uk).

Y. Ivanenko was with the Department of Physics and Electrical Engineering, Linnaeus University, Växjö, Sweden. He is now with the Department of Mathematics and Natural Sciences, Blekinge Institute of Technology, Karlskrona, Sweden. (e-mail: yevhen.ivanenko@bth.se).

S. Nordebo is with the Department of Physics and Electrical Engineering, Linnaeus University, Växjö, Sweden. (e-mail: sven.nordebo@lnu.se).

T. W. Rademacher in with Emergex Vaccines Holding Ltd, Abingdon, OX13 6BH, UK. (e-mail: twr@emergexvaccines.com).

A. Demosthenous, N. Neshatvar, and Y. Wu are with the Department of Electronic and Electrical Engineering, University College London, London, UK. (e-mail: a.demosthenous@ucl.ac.uk).

gold core less than 2 nm do not have any measurable plasmonic, which is required to image them [10]. MRI can also use a contrast agent in the form of gadoterate meglumine (Gd-DOTA) but this is not ideal as a scaffold to create new drugs. GNPs are more suited as a scaffold to create new drugs, but unfortunately, MRI cannot use them, as they are not magnetic and cannot be seen in the MRI. PET, CT and MRI produce static images unlike the new method proposed in this paper that can produce dynamic images in real-time.

A. GNPs as Contrast Agents

GNPs are more suited as a scaffold to create new drugs and can be used as contrast agents to track particular physiological processes during imaging. Particles below 5 nm diameter including the attached ligands can be cleared rapidly by the body's reticuloendothelial system following injection into the bloodstream. Methods based on plasmonic GNPs for cancer diagnosis and photothermal therapy are being investigated, due to the optical properties. The surface plasmon resonance (SPR), a unique phenomenon to plasmonic (noble metal) nanoparticles produces a strong electromagnetic field on the particle surface and enhances all the radiative properties such as absorption and scattering. The heating efficiencies and spectral ranges vary with the type of nanoparticle. However, for GNPs with attached ligands that have a core of size below 2 nm, there is no phenomenon to plasmonic resonates [11] which is in the size range currently being developed for immunotherapy. GNPs are more suited as a scaffold to create new drugs, but unfortunately, MRI cannot use them, as they are not magnetic and cannot be seen in MRI.

Previous research suggested that GNPs has the potential as a contrast agent for bioimpedance measurements [12] and it is possible to detect cancer cells based on the impedance increase [13]. However, the addition of GNPs to decrease impedance in cancer cells would limit the ability to distinguish between GNPs and cancer cells.

B. Bioimpedance Imaging

To address this, we have created an imaging system using quantum cluster GNPs [10] as contrast agent, activated with radio frequency (RF) fields to heat the functionalized GNPs, causing a change in impedance around them. This change is then identified with electrical impedance tomography (EIT). EIT is a non-invasive, radiation free technique that images an object by injecting small sinusoidal currents through electrodes on its boundary, and measures the resulting potentials developed on the same or other electrodes. This process permits the estimation of the distribution of the inner conductance (impedance) of the object with high temporal resolution (~120 images per second [14]. Clinical studies have already been undertaken demonstrating in potential for use on humans [15]. A clinical study of 200 neonates for 72 hours each was undertaken during the CRADL project [cradlproject.org].

EIT is sensitive to temperature changes causing the impedance to change [16]. This allows the creation of images of temperature changes. Also, multifrequency EIT which is based on the principle of electrical impedance spectroscopy [17] can provide images of cancer regions based on the structure of the cells. It would allow this new method to provide an image of the tumor cells and the location of the immune system drug [18].

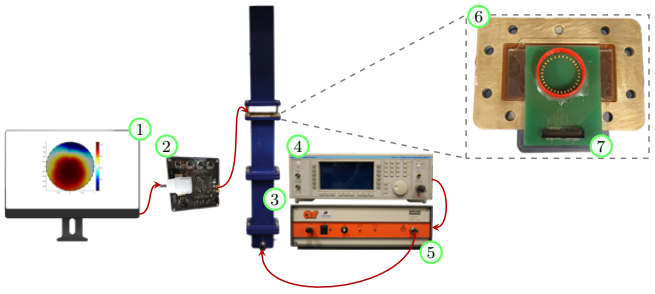

Fig. 1. Schematic of the experimental set-up. The set-up consisted of the EIT system (2) which was connected to the 32-electrode PCB (7) placed inside the waveguide (3), on the Kapton window (6). The waveguide (3) was driven by the RF signal generator (4) and powered by the amplifier (5). All the images recorded by the EIT system (2) were observed via the display (1).

This paper presents of a novel EIT method to locate nanoparticles below 5 nm diameter in human tissue. This new approach has a number of advantages in comparison with other methods that are currently used to locate GNPs in human tissue. The rest of this paper is organized as follows. Section II provides the methods for the imaging system and the cell models. In Sections III and IV, the obtained results are presented and discussed, respectively. Section V provides concluding remarks with promising directions for future research.

II. Method and Materials

A. Optimal Frequency for GNP Heating

Experiments have already demonstrated that GNPs can be heated with RF [19], [20], [21] [22]. The size and the biological material (ligands) attached to the nanoparticle changes the frequencies at which heating is obtained [23]. To address this and to identify an optimal frequency for GNP heating for further experimentation, we considered the frequencies where the lowest heating rate of the solution based only on the medium (PBS) occurred. Furthermore, we considered the frequencies where the heating rate of the solution that contained GNPs was sufficiently higher than the rate of the PBS-based solution. From a practical point of view, these criteria prevent the risk of human tissue damage during the therapy.

In this experiment, for frequencies between 2.265 GHz and 2.7 GHz, eppendorfs containing 1.5 ml of PBS and Citrate stabilized GNPs (GNP-CS) solutions, respectively, were placed one by one in the waveguide, on the Kapton film, see Fig. 1. The waveguide setup was driven by a Marconi Instruments 2031 RF signal generator at 0 dBm for 30 minutes, and the temperature of the solutions was measured with fast immersion probes [24] connected to a Luxtron 812 fiber optic thermometer.

B. RF System and Waveguide

The PCB-unit was mounted on a WG10 waveguide that was

custom designed with a cut-off frequency range of 2.07 GHz to 4.15 GHz (Global Invacom Waveguide, UK). The waveguide consisted of four main parts: a 320 mm fixed load, two 200 mm precision straights and a coaxial adaptor; all made of silver-finished brass. A pressure flange fitted with a Kapton window was used to stabilize the system and was fitted with a transparent 3D-printed holder to keep the samples in place. The waveguide was driven by a signal generator (Marconi Instruments 2031 RF signal generator, operating from 10 kHz to 2.7 GHz) at 0 dBm which was amplified by a 5-Watt power amplifier. The power amplifier could provide a maximum power of 5 W in the frequency range of 800 MHz to 4.2 GHz (Amplifier Research model 5S1G4, USA).

C. EIT System

The system used for EIT imaging is the Pioneer set from SenTec AG [25]. It consists of an advanced interface with 32 channels, a smart sensor belt connector, a power supply unit and data communication documentation. The system is capable of injecting programmable currents from 1 mA to 7 mA peak in the frequency range of 50 kHz to 250 kHz. It can provide different data frame rates per second (fps). The SenTec EIT monitor software (STEM) allows setting of EIT parameters such as excitation frequency and injection current. It provides real-time monitoring of the signals and continuous quality checks of each one of the electrodes. The raw data can be stored for post-processing and signal analysis. Unless stated otherwise, all experiments were recorded at 1 fps; the injected current was 7 mA at 250 kHz. The raw data extracted was analyzed in MATLAB and EIDORS software [26] to reconstruct the images. The reconstruction algorithm was based on difference imaging with respect to the reference image by using GREIT algorithm [27]. All measurements were recorded for 7 minutes; during the first 2 minutes the power amplifier was off. The images from this period were used as the reference. Then the power amplifier was turned on for 5 minutes while continuous live monitoring of the samples was recorded.

A cell model was created consisting of colon epithelial and colorectal cancer cells with GNPs in cancer cells. This cell model was placed in a custom-made ring of 32 gold-plated electrodes of size 1 mm × 1.5 mm utilized to be interfaced with the EIT system (see the structural representation of the EIT-based system in Fig. 2). A well of 2.9 cm diameter, 1 cm height and 1 mm thickness was designed and placed onto the PCB-unit to contain the samples within the electrode ring during the experiments. Each electrode was connected to the EIT system by a ribbon cable.

D. Preparation and Analysis of GNP

GNP-CS were used with a core size of 5 nm diameter and mass concentration of 0.06 mg/mL (NP01-0051010, ClineScientific, UK [28]) and an optical density of 1. The hydrodynamic diameter and SPR peak for these GNP-CS were verified and confirmed via dynamic light scattering (DLS) and ultraviolet-visible spectroscopy (UV-vis), respectively. The GNP-CS were purified with centrifugal filter units (Amicon® Ultra-15, cut-off 10kDa), and re-suspended in phosphate-buffered saline (PBS) (DPBS 1X Gibco™, ThermoFisher, UK) 7.17 pH before use.

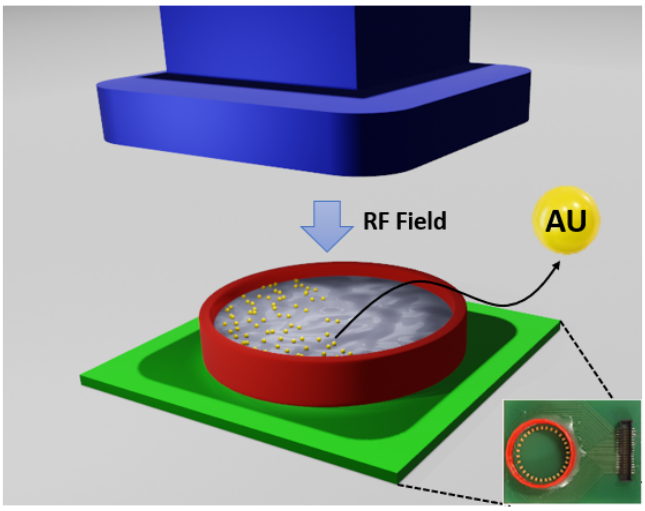

Fig. 2. Structural representation of the EIT-based imaging system consisting of a ring of 32 gold-plated electrodes of size 1 mm × 1.5 mm utilized to be interfaced with the EIT system. A well of 2.9 cm diameter, 1 cm height and 1 mm thickness is placed onto the PCB-unit.

GNPs stabilized with glutathione (GSH) were synthesized by adapting a similar method [29]. Briefly, 0.01 mM of tetrachloroauric acid ($HAuCl_4.3H_2O$) was dissolved in 10 mL of DiH_2O, to which a freshly prepared sodium borohydrate ($NaBH_4$) solution (0.015mM) was added dropwise, stirring at 25 ˚C until the solution color changed to deep red. Then, 50 µl of glutathione (GSH, 0.2 mM) was added and stirred for 1 hour. The free GSH molecules were removed by centrifugation with 10 kDa centrifugal filter units.

The stock GNP-GSH solution was used to produce folic acid functionalized GNPs (GNP-FA) via 1-(3-dimethylaminopropyl)-3-ethylcarbodiimide hydrochloride-N-hydroxysuccinimide (EDC-NHS) linkage. 10 mL of stock GNP-GSH solution, 25 µl of EDC (50 mM) and 25 µl of NHS (50 mM) were added, stirred for 1 hour before adding folic acid (0.01 mM), and stirred overnight. Unbound folic acid was removed with centrifugal filter units (Amicon® Ultra-15, cut-off 30 kDa) and the GNP-FA solution was kept at 5 ˚C until needed. Folic acid binding was confirmed via UV-vis (FLUOstar Omega, BMG Labtech, Germany) and DLS (Zetasizer Nano ZS, Malvern Panalytical, UK) studies. The concentration of folic acid bound to the GNPs was calculated to be 1.1×10^{-4}M, through Beer-Lambert law ($A = \varepsilon lC$); FA extinction coefficient ε=15,760$M^{-1}cm^{-1}$, path-length $l = 1$ cm, and absorbance $A = 1.736$.

For cell uptake detection, fluorescein isothiocyanate (FITC) was added to stock GNP-FA solution at 0.1 M concentration and allowed to react overnight in an orbital shaker, at room temperature, in the dark. Unbound FITC was removed via centrifuging as previously described. Deionized water used throughout experiments was maintained at >1 MΩ with a lab deionization unit (Select Analyst, SUEZ Water Technologies & Solutions, France).

E. Influence of RF Field on Citrate GNPs

To increase the concentration of the stock GNP-CS solution, 1 mL aliquots ($3.21 \cdot 10^{-4}$M) were filtered with centrifugal filter units and the obtained pellets kept at 4 °C. PCB-units containing either 2 mL PBS or 1.9 mL PBS were placed one at the time on the waveguide as shown in Fig. 1. The PCB-unit containing 1.9 mL PBS, the 100µl pellet of GNP-CS was pipetted in the center of the electrode ring before the reference was recorded. Each RF experiment was recorded with the EIT system as described previously. UV-vis spectra were recorded to confirm the GNPs did not aggregate following RF excitation.

F. Cell Lines and Culturing

Human Duke's B Colorectal Cancer (CRL2159, ATCC no. LS411N) and colon epithelial (CRL1790, ATCC no. CCD841) cell lines were obtained from LGC Standards-ATCC. CRL2159 and CRL1790 were cultured with RPMI-1640 (product no. R8758) and MEM (product no. M4655) respectively, both containing 10% foetal bovine serum and 1% pen-strep solution. Cells were maintained inside an incubator with humidified atmosphere containing 5% CO_2 at 37 °C.

G. In-Vitro Uptake Studies

After culturing CRL2159 and CRL1790 as mentioned above, both were trypsinized. Approximately 10,000 cells of each cell line were pipetted onto separate sterilized 13 mm diameter cover-slips placed in separate 6-well plates, covered with medium and maintained in the incubator to reach 80-90% confluence (final cell count CRL1790 = 1.15×10^5 and CRL2159 = 1×10^6 per cover-slip).

To visualize folate receptor alpha (FR-α) expression, plates with each cell line were washed 3 times with PBS and fixed with 4% paraformaldehyde (PFA) for 30 minutes. Residual PFA was washed twice with PBS, followed by treating the fixed cells with citrate buffer at pH 6 for 10 minutes. After washing, the cells were treated with 50% horse serum in PBS (1:1), followed by incubation with 1:100 concentrated FR-α rabbit polyclonal antibody (PA5-42004, Thermofisher) for 90 minutes. The cells were further incubated after washing with biotinylated-secondary antibody (VECTASTATIN ABC kit, Vector laboratories Ltd, UK) for 30 minutes. Finally, the cells were incubated with tertiary peroxidase-labelled avidin for 20 minutes before developing with a tyramide signal amplification (TSA) fluorescein system (NEN Life Science, USA). After washing again with PBS, the cover-slips were mounted onto slides using DAPI (4′,6-diamidino-2-phenylindole) based mounting media (VECTASHIELD®, Vector laboratories Ltd, UK). FR-α expression was visualized with a Leica TCS SP2 confocal microscope.

To visualize GNP internalization, plates with each cell line were incubated with 400 µl of FITC bound GNP-FA at 1×10^{-7} M concentration for 3 hours. The media was discarded, and any non-bound GNP-FA washed away with PBS. The cells were fixed with PFA for 30 minutes, followed by mounting and visualization as described above.

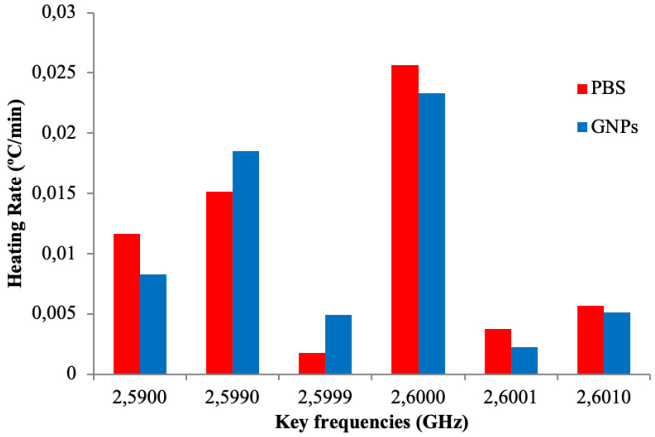

Fig. 3. The heating rate difference between PBS and GNP-CS solutions during 30 minutes exposure at different frequencies. The figure contains only *the key frequencies* at which the heating rate of GNPs is either close or higher than the heating rate of PBS.

H. Influence of RF on GNP Incubated CRL2159

Cover-slips containing CRL2159 cells were prepared as above and maintained in the incubator. Cells were incubated with 400ul of either RPMI, GNP-CS ($3.21 \cdot 10^{-4}$M) or GNP-FA ($3.21 \cdot 10^{-4}$M) for 3 hours. After which the media was discarded, cells washed with PBS and covered with fresh RPMI until use. Each cover-slip was placed in a PCB-unit, covered with 1 mL RPMI and placed inside the waveguide. After a brief period of acclimatization, each PCB-unit was placed inside the waveguide and the RF exposure recorded as described previously.

III. Results

A. Optimal Frequency for GNP Heating

As an optimal frequency for heating GNPs, we consider a frequency, at which the following phenomena are observed: (1) the heating rate of the background is low, i.e., we expect that human tissue will not be damaged at the optimal frequency; (2) GNPs are expected to be heated when condition (1) takes place, and the heating rate of nanoparticles is higher than the heating rate of the surrounding medium. Fig. 3 shows results on heating rate of PBS and GNP-CS solutions that have been excited for 30 minutes at different frequencies in the microwave regime. Note that the results are demonstrated only for frequencies at which the heating rate of GNPs is higher than the heating rate of PBS, and for the initial frequencies (lower and higher) where this observation shifted toward higher heating rate of PBS. Over the remaining part of the frequency band (2.265 GHz, 2.7 GHz), PBS rate of temperature change was consistently higher than that of the GNP solution. Furthermore, there was no linear correlation observed between the rates of temperature increase.

B. Analysis of Synthesized GNPs

UV-vis and DLS analyses were performed to confirm the synthesis of GNPs-GSH, as well as to confirm the subsequent attachment of folic acid (FA) to the GNPs. Fig. 4 shows the absorption spectra for GNPs-GSH with no SPR peak at 520 nm as expected from particles <2 nm, where a peak was seen after

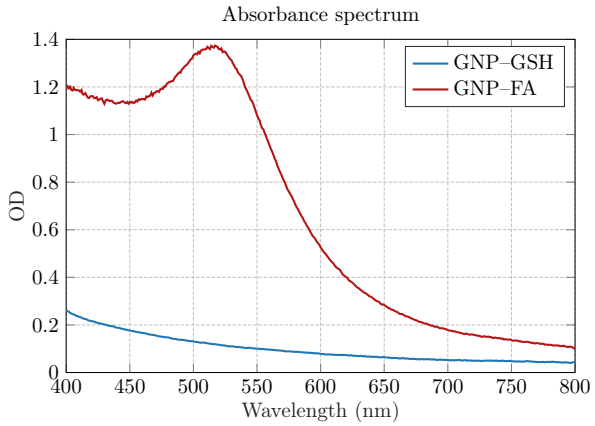

Fig. 4. UV-vis absorbance spectra obtained from synthesis of GNP-GSH and after functionalization with folic acid – GNP-FA.

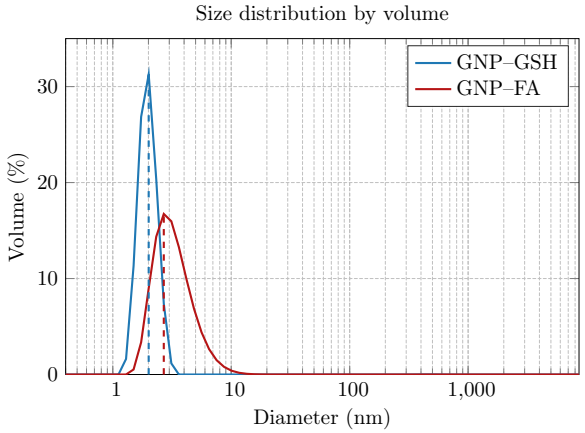

Fig. 5. Size distribution obtained via analysis of GNP-GSH synthesis and after FA functionalization.

FA addition, confirming the synthesis of GNPs-FA. The size obtained from DLS quantified the size of GNPs-GSH to 1.9±0.3 nm and GNPs-FA to 3.4±1.4 nm and confirmed a narrow size distribution of the synthesized particles; see Fig. 5.

C. *Locations of GNPs in Solution With EIT*

Fig. 6 shows the EIT image reconstructions obtained after exposing PBS (Fig. 6(a)) and PBS with added GNP-CS (Fig. 6(b)) to a RF field. Both solutions were recorded for 1 minute without an active RF field to establish the reference, followed by exposure to RF at 2.5999GHz for 5 minutes. To avoid complete homogenisation of the GNPs with PBS, the aliquot was added just before taking the reference, as shown in Fig. 6(c)).

Difference imaging of the PBS solution showed a slight change of colour, with a calculated change of 25%. Adding the GNP-CS aliquot to a fresh PBS solution gave around 80% of change in the EIT image. Twenty repeats for both samples were made, using fresh solutions for each measurement, provided a standard deviation of <0.4% for PBS and with added GNP-CS a standard deviation about 4.37%; see Table I.

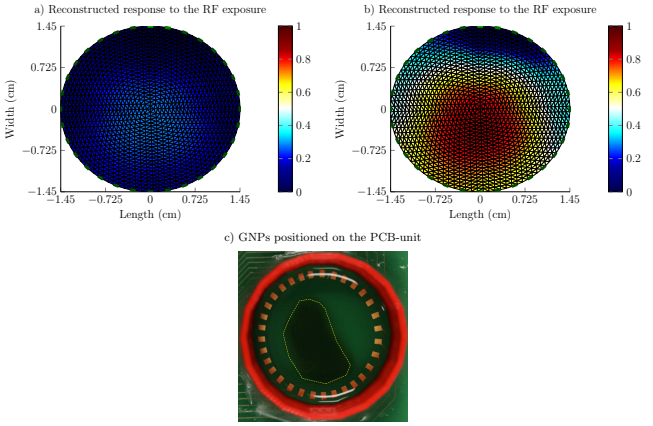

Fig. 6. EIT reconstructed images obtained after exposing PBS (a) and PBS with added GNP-CS (b) to a RF field. The position of GNP-CS on the PCB-unit is depicted in (c). Both solutions were recorded for 1 minute without an active RF field to establish the reference, followed by exposure to RF at 2.5999 GHz for 5 minutes.

TABLE I
MEAN-VALUE PERCENTAGE CHANGE AND STANDARD DEVIATION OF RESULTS OBTAINED FROM EIT OF PBS AND PBS+GNPS

Solution	Mean Value (%)	Standard Deviation (%)
PBS	24.961	0.338
PBS + GNPs	80.163	4.369

D. *In-Vitro Uptake Studies*

Confirming the internalization of GNPs into the colorectal cancer cells was undertaken in order to compare them with the EIT images. GNP-FA were further functionalized with FITC, a fluorescent moiety, which allowed simple visualization with confocal microscopy [30]. FITC used in the experiments has a reactive isothiocyanate group that can react and bind with amine and sulfhydryl groups. It had reacted with amine group in glutathione and bonded with it and in turn signals folic acid bound to GNPs in the cells *in vitro*. Colorectal cancer cells (CRL2159) were chosen due to over-expression of folate receptors around their surface and were cultured using standard practices, along with colon epithelial cells (CRL1790), in order to assess the differences in internalization with cells which do not present folate receptor [31], [32]. The *in vitro uptake studies* were carried out separately on both cell lines since use of different media prohibits co-culturing; besides cancer cells compete for the nutrition in the media starving normal cells [33]. In order to confirm folate receptor alpha expression, anti-FR-α antibodies were used to target the receptors, while the biotin-avidin interaction of secondary and tertiary antibodies enabled their visualization. Fig. 7 shows images resulting from immunocytochemistry staining and confocal imaging of CRL1790 and CRL2159 cells. CRL1790 cells (Fig. 7(a)) shows no evidence of the green fluorescent signal expected for the receptors, while showing clear defined nuclei in blue, from DAPI counter-staining. A strong green fluorescent signal was present for CRL2159 cells (Fig. 7(b)), which shows strong over-expression of FR-α receptors.

Both cell lines were incubated with GNP-FA ($1 \cdot 10^{-7}$ M) for

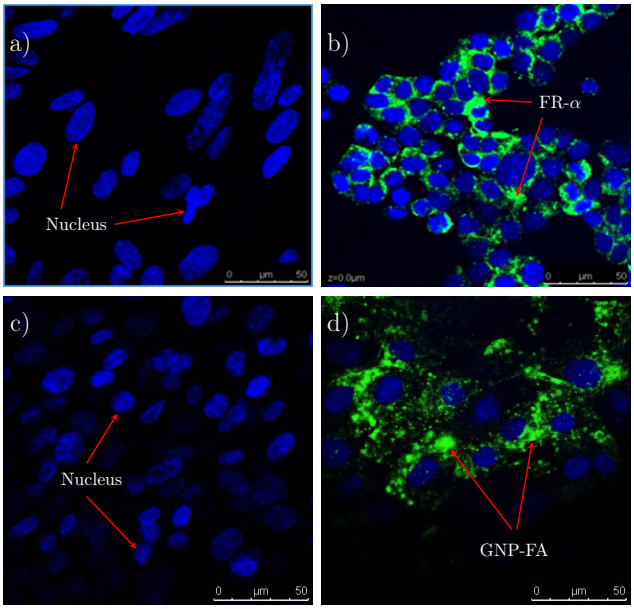

Fig. 7. Shows the expression of FR-α receptors in colorectal cancer cells [(a) and (b)] and GNP-FA internalisation [(c) and (d)] using a confocal microscope. Scale bar = 50 µm. Magnification 40X. (a) human colon epithelium cells showing negative expression for FR--α receptors (b) colorectal cancer cells showing positive expression for FR--α receptors (in green) (c) human colon epithelium cells showing no GNP-FA internalisation (d) colorectal cancer cells showing internalization of GNP-FA (in green).

TABLE II
MEAN-VALUE PERCENTAGE CHANGE AND STANDARD DEVIATION OF RESULTS OBTAINED FROM EIT OF CANCER CELLS, WITH OR WITHOUT GNP INCUBATION

Solution	Mean Value (%)	Standard Deviation (%)
CRL2159	7.944	0.395
CRL2159 + GNPs-CS	17.220	1.303
CRL2159 + GNPs-FA	39.753	2.014

3 hours, after which any non-bounded nanoparticles were washed off before fixing and staining the cells to evaluate the presence of GNPs in the colorectal cancer cells. The nuclei were counterstained with DAPI and stained blue while any present GNP-FA would show green, fluorescent staining. Here, internalization is showed indirectly by the fluorescence quenching mechanism. Due to the small SPR wavelength of the GNPs, as long as glutathione-folate ligand was conjugated with GNPs, fluorescent remained quenched. However, upon internalization in the cell the ligands on the GNPs surface displaces which leads to no fluorescent quenching and visualization of the displaced glutathione-folate ligand. Fig. 7 shows the confocal images obtained for colon epithelial cells (Fig. 7(c)) and colorectal cancer cells (Fig. 7(d)). It is evident from the Fig. 7(c) that no GNP-FA were internalized by the colon epithelial cells, whereas colorectal cancer cells show strong fluorescent signals in the cell cytoplasm indicating the presence of internalized GNP-FA [34].

E. Visualization of GNPs in Colorectal Cancer Cells Using EIT

Coverslips containing colorectal cancer cells were incubated

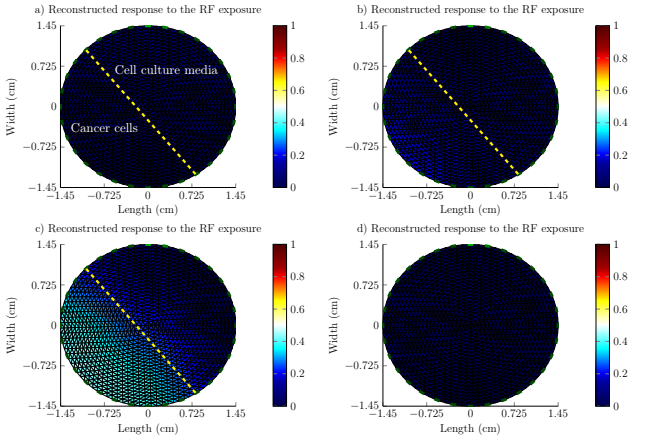

Fig. 8. Human colorectal cancer cells grown in cell culture media, were incubated with (a) no GNPs, (b) GNP-CS solution, (c) GNP-FA solution. After RF exposure for 5 minutes, EIT reconstruction was obtained. Dashed line represents the area covered by CRL2159 cells, occupying ~40 % of well area. (d) CRL1790 normal colon epithelium cells after RF exposure. The color bar represents the normalized values as percentage change from dark blue (0%) to red (100%).

with culture media, GNP-CS, or GNP-FA. Once the reference was taken, all sets were exposed to an RF field for 5 minutes (temperature change less than one degree) and the resultant EIT images are shown in Figs. 8(a)-(c). Images obtained with colorectal cancer cells and no added GNPs showed a very slight change of color and the difference to the reference was calculated to around 8%. When incubating the cells with citrate-coated GNPs the change after RF exposure increased to 18%, and the area where cells were located was slightly brighter than the remaining area. When the cells were incubated with functionalized GNPs (GNP-FA), the change of color was more apparent and was calculated to approximately 42%. This change reflected on the EIT image as the cell area was more clearly identifiable from the rest of the area. In order to confirm the changes seen in the EIT images were not due to artefacts, the experiment was repeated twenty times, from incubation to visualization. Repeats without added GNPs demonstrated a standard deviation about 0.34%, while repeating the EIT recording with GNP-CS or GNP-FA provided a standard deviation below 3%; see Table II.

Human normal colon epithelium cells were incubated with culture media only and exposed to an RF field for 5 minutes as negative control for EIT cell damage. The images obtained showed negligible changes to the reference of around 6%; see Fig. 8(d).

IV. DISCUSSION

When the nanoparticles within the cancer cells are stimulated with the RF-field, they produce a small change in temperature (less than one degree). The temperature difference corresponds to an impedance change due to the disruption of ions flowing in the cells. Since the reconstructed EIT images produce a difference image based on the pre and post RF stimulation of the nanoparticles, this enables us to estimate the location of the GNPs. Furthermore, the approach can be repeated to identify whether the location of particles has been changed.

When the nanoparticles are excited by the RF-field, they produce a faster rate of temperature change of cells and tissue at certain frequencies than untreated cells and tissue, i.e. those that do not contain nanoparticles. In the example presented in this paper, the frequency 2.5999 GHz was chosen. Even if the excitation causes direct heating of the cells and tissue, the faster rate of heating by the nanoparticles generates a temperature difference that can still be imaged by EIT. Thus, the location of the nanoparticles is indicated by a 'hot-spot' in the EIT image.

A. Choice of Frequency

It was observed that at frequencies 2.265 GHz, 2.599 GHz, and 2.5999 GHz, the GNP-based solution provided a heating rate higher than the solution based on PBS. However, despite the larger observed temperature increases of the GNP-CS solution higher at frequencies 2.265 GHz and 2.599 GHz, the smallest rate increase in the PBS solution was achieved at 2.5999 GHz, which corresponds to the case of the lowest elevation of temperature in a human tissue and consequently, the lowest risk to damage it. Furthermore, the lowest rate in the tissue provides a possibility to avoid impedance changes in the corresponding regions, which will improve accuracy results provided by the EIT system. Thus, 2.5999 GHz was consequently chosen as the optimal frequency for GNP heating in the further experiments.

The efficiency of the method for determination of an optimal frequency for GNP heating results in Fig. 6. Figs. 6(a)-(b) shown the reconstructed EIT images of two different solutions, which were placed on the PCB-unit, as shown in Fig. 6(c), and excited at 2.5999 GHz. Comparing the obtained results, it should be noted when GNPs are added to the solution, the response to the electromagnetic field excitation at 2.5999 GHz is higher in nanoparticles than in the surrounding PBS medium, which validates a correct frequency choice.

However, identification of the optimal frequency for GNP heating based on temperature measurements is time consuming and does not provide information over a large frequency interval. As an alternative approach, for future work, an optimal frequency for GNP heating can be identified based on the highest absorption coefficient over a given frequency interval for a solution placed in a waveguide. The absorption coefficient can be determined by the law of conservation of energy, where the energy balance is given by $A = 1 - R - T$; A denotes the absorption coefficient, R and T are the reflection and the transmission coefficients, respectively, which can be measured.

B. EIT of GNPs in Solution

When stabilized GNPs are added to a solution, they will disperse rather than aggregate, and that makes accessing their response independently of the solution more difficult. As it was necessary to analyze how the GNPs respond to radio frequency exposure, their storage solution, PBS, was also tested independently. An aliquot of GNPs was separated from the PBS by centrifugation and added to fresh PBS just before experimentation, in order to limit dispersion. PBS was added to two 32-electrode PCB boards, adding a pellet of GNPs to only one of them. Both boards were placed in the waveguide, recording a reference before exposing both solutions to RF for 5 minutes. Fig. 6 shows the images produced from the EIT recording, after exposure, where the difference between the PBS solution (Fig. 6(a)) and the PBS plus GNP-CS (Fig. 6(b)) is apparent. The PBS solution showed a change from the reference of around 25%, representing a small change in image contrast on the reconstructed image, and a standard deviation below 0.4% for twenty repeats. Adding the GNP-CS aliquot to the PBS solution caused a recorded difference on average of 80% and enhanced contrast on the resulting image. From the two obtained images it is apparent that the GNPs are more greatly affected by the RF exposure than their surrounding medium, being consistent with the real position of the GNPs inside the PCB well. Fig. 6(c) shows the GNP aliquot after 5 minutes of being added in the PBS solution, and while the dispersion of the GNPs cannot be controlled, it correlates with the EIT image produced. Although from the produced EIT images the borders of the GNP aliquot cannot be defined, the presence of the nanoparticles can easily be identified. The uncontrolled dispersion of the GNPs could also explain the standard deviation of 4.37% for twenty repeats of the experiments, as shown in Table I.

C. Confocal Confirmation of GNPs Targeting Colorectal Cancer Cells

Targeting cancer cells through overexpressed receptors located on the cell's surface is a widely utilized method of cancer cell identification. Folate receptors are found overexpressed in a large variety of cancer cell types whereas healthy cells are much less likely to express these receptors. Colorectal cancer cells overexpress folic acid receptors while colon epithelium cells have a weak expression of these receptors, and thus targeting folate receptors can be used to differentiate between cancerous and healthy colorectal tissue. Immunocytochemistry was used to image folate receptors on both cell lines, in order to confirm overexpression (Fig. 7). Confocal imaging of colon epithelium cells (Fig. 7(a)) showed absence of anti-FR-α antibodies indicating this receptor was absent or minimally expressed in normal colonic cells. In contrast, colorectal cancer cells (Fig. 7(b)) presented a strong fluorescent signal indicative of FR-α overexpression. For both cell lines, horse serum was used to inhibit any unwanted signals and non-specific binding of primary antibodies to the antigen receptors. The resulting images confirmed that folate receptors could be used to differentiate normal and cancer cell lines.

GNPs were functionalized with folic acid, and to allow simple confocal microscopy visualization, the GNP-FA constructs were labelled with FITC [36]. In order to assess the targeting ability, CRL1790 and CRL2159 cells were incubated with the FITC labelled GNP-FA construct and prepared for confocal microscopy. Fig. 7 shows the resulting images for both cell lines where the cells nuclei were counterstained using DAPI mounting media and stained blue. In colon epithelium cells (Fig. 7(c)), well-defined nuclei can be identified, and no green fluorescence is present, suggesting a lack of GNPs. However, in colorectal cancer cells (Fig. 7(d)), particles emitting strong green fluorescence are present in the cell's cytoplasm, indicating GNP-FA internalization. The fluorescent particles are associated with the internalization of the GNPs

inside the cytoplasm via receptor-mediated endocytosis (RME) [35].

D. EIT of GNPs Incubated with Cells

To confirm the ability of EIT to detect GNPs against a complex surrounding, colorectal cancer cells were incubated with cell culture media, with GNP-CS, or with functionalized GNPs (GNP-FA). Fig. 8 shows the EIT images obtained after 5 minutes RF exposure. When incubated without any GNPs, the CRL2159 cells did not produce a discernible change on the EIT image, and the change to reference was calculated to around 8%. This was expected as the cells themselves do not suffer great changes during the short time period, and no changes in the surrounding medium are expected either, which confirms the weak interaction with the RF-field. Twenty experiments were repeated with a standard deviation <1%. Colorectal cancer cells incubated with citrate-coated GNPs produced a larger change in the EIT recording (around 18%) however the change was not enough to create contrast against the medium, contrary to what was seen previously with these GNPs in PBS. Since the cells were washed after incubation and before RF exposure in order to remove any unbound GNPs, and the GNP-CS were not functionalized, it was expected that the number of GNPs remaining in the cells would be greatly diminished, and thus this small change was expected. The cells incubated with GNP-FA showed a greater change compared to the previous images, with approximately 40±2% (20 repeats of the experiment) change from reference. This change was reflected in the EIT image as the cell area was more clearly identifiable from the rest of the PCB area. The GNP-FA have been previously shown to be internalized by the colorectal cancer cells and thus were expected to remain in greater numbers after the wash steps. The change in impedance caused when GNPs were exposed to the RF field could be used to locate the CRL2159 cells' position inside the PCB board, as it was comparable to the original placement of the cover slips. Repeating the experiment with both GNP solutions provided a standard deviation less than 3% (see Table II), which could be due to environmental temperature changes or to the washing process. No difference was observed between no exposure to RF and after exposure to RF, which confirms that GNP-FAs were not taken up in normal cells (Fig. 8(d)). GNP-FA should not be absorbed by the normal cells as they are designed to only target cancer cells.

Since the PCB material does not allow for cells to be grown directly on its surface, this study was limited by the amount electrode area which could be covered with cells for GNP incubation. The cells were placed at the edge of the PCB well, the area covered by the cells towards the lower left corner of the image. The aim of this study was to show that changes occurring from exposing GNPs to an RF field at a frequency could be used to locate and create an image in cancer cells.

V. Conclusion

In this paper, a new method for location of functionalized gold nanoparticles using EIT has been presented. It demonstrated that functionalize GNPs in colorectal cell line can be located and validated with sufficient contrast change in the EIT images with RF stimulation. Images of impedance changes around 80±4% was found for a sample of citrate stabilized GNPs in PBS solution. It was also demonstrated that colorectal cancer cells incubated with culture media, with internalisation of GNPs into the colorectal cancer cells, resulted in an impedance change of approximately 40±2%. This change was reflected in the EIT image as the cell area was more clearly identifiable from the rest of the area. The demonstrates EIT can locate clusters functionalised GNPs (with core sizes below 2 nm) in human cells by imaging the change in impedance before and after the GNPs have been stimulated by RF.

The limit of GNPs detected through EIT is conditional on RF power. Furthermore, it is predicted that the amount of GNPs required to image in *in vivo* conditions varies from 2D cell culture conditions. Therefore, future work will seek to calculate the limit of detection of the technique in an animal model.

Future work will also focus on developing a system for an animal model to validate the new imaging approach and it is hoped that this will lead to a system that can be used on humans for locating nanoparticle-based drugs. The results in this paper demonstrate the potential of this new methods to provide images of GNPs in the tumor cells. Furthermore, the proposed system can potentially be used with iron-oxide nanoparticles [36]. However, the size of these particles is larger than 5 nm in diameter.

References

[1] J. Patra, G. Das, L. Fraceto, E. Campos, M. Rodriguez-Torres, L. S. Acosta-Torres, L. Diaz-Torres, R. Grillo, M. Swamy, S. Sharma, S. Habtemariam and H. Shin, "Nano based drug delivery systems: recent developments and future prospects," *J. Nanobiotechnology*, vol. 16, pp.1-33, 2018.

[2] A. Mikhail, A. Partanen, P. Yarmolenko, A. Venkatesan and B. Wood, "Magnetic resonance-guided drug delivery," *Magn. Reson. Imaging Clin. N. Am.*, vol. 23, p. 643–655, 2015.

[3] S. Chen, H. Liu, C. Xiong, L. Zhan, J. Sun and Z. Nie, "Mass spectrometry imaging of the in situ drug release from nanocarriers," *Advances Science*, vol. 4, no. 10, 2018.

[4] R. Mortishire-Smith, D. O'Connor, J. Castro-Perez and J. K. Kirby, "Accelerated throughput metabolic route screening in early drug discovery using high-resolution liquid chromatography/quadrupole time-of-flight mass spectrometry and automated data analysis," *Rapid Commun. Mass Spectrom.*, vol 19, pp. 2659-2670, 2005.

[5] R. Chakravarty, H. Hong and W. Cai, Positron emission tomography image-guided drug delivery: Current status and future perspectives," *Mol. Pharm.*, vol. 11, no. 11, pp. 3777−3797, 2014.

[6] L. Arms, D. Smith, J. Flynn, W. Palmer, A. Martin, A. Woldu and H. Susan , "Advantages and limitations of current techniques for analyzing the biodistribution of nanoparticles," *Front. Pharmacol.*, vol. 9, 2018.

[7] A. Buchberger, K. DeLaney, J. Johnson and L. Li, "Mass spectrometry imaging: A review of emerging advancements and future insights," *Anal Chem.*, vol. 90, no. 1, pp. 240–265, 2018.

[8] X. Liu and A. Hummon, "Mass spectrometry imaging of therapeutics from animal models to three-dimensional cell cultures," *Anal Chem.*, vol. 87, no. 19, pp. 9508–9519, 2015.

[9] M. Shilo, T. Reuveni, M. Motiei and R. Popovtzer, "Nanoparticles as computed tomography contrast agents: Current status and future perspectives," *Nanomedicine,* vol. 7, no. 2, pp. 257-69, 2012.

[10] C. Kumara, X. Zuo, D. Cullen and A. Dass, "Faradaurate-940: synthesis, mass spectrometry, electron microscopy, high-energy X-ray diffraction, and X-ray scattering study of Au∼940±20(SR)∼160±4 nanocrystals," ACS Nano., vol. 8, no. 6, pp. 6431–6439, 2014.

[11] S. Kumar and R. Jin, "On the optical absorption properties of quantum-sized gold nanoclusters," *J. Nanoscience Letters*, vol. 3, no. 22, pp. 1-5 2013.

[12] M. Callaghan, T. Lund, P. Hashemzadeh, I. Roitt and R. Bayford, "An investigation of the impedance properties of gold nanoparticles," *J. Phys.: Conf. Ser.*, vol 224, p. 012058, 2010.

[13] A. Pathiraja, P. Ziprin, A. Shiraz, R. Mirnezami, A. Tizzard, B. Brown, A. Demosthenous and R. Bayford, "Detecting colorectal cancer using electrical impedance spectroscopy: an ex vivo feasibility study," *Physiol. Meas.*, vol. 38, no. 6, pp. 1278-1288, 2017.

[14] Y. Wu, D. Jiang, A. Bardill, R. Bayford and A. Demosthenous , "A 122 fps, 1 MHz bandwidth multi-frequency wearable EIT belt featuring novel active electrode architecture for neonatal thorax vital sign monitoring," *IEEE Trans. Biomed. Circuits. Syst.*, vol. 13, no. 5, 927-937, 2019.

[15] M. Kallio, M. Rahtu, A. van Kaam, R. Bayford, P. Rimensberger and I. Frerichs , "Electrical impedance tomography reveals pathophysiology of neonatal pneumothorax during NAVA," *Clin. Case Rep.*, vol. 8, no. 8, pp. 1574-1578, 2020.

[16] J. Edd, L. Horowitz and B. Rubinsky, "Temperature dependence of tissue impedivity in electrical impedance tomography of cryosurgery," *IEEE Trans. Biomed. Eng.*, vol. 52, no. 4, pp. 695-701, 2005.

[17] R. Bayford and A. Tizzard , "Bioimpedance imaging: an overview of potential clinical applications," *Analyst*, vol. 137, no. 20, pp. 4635-4643, 2012.

[18] Y. Mi, T. Hagan, B. Vincent and A. Wang., "Review, emerging nano-microapproaches for cancer immunotherapy," *Adv. Sci. (Weinh)*, vol. 6, no. 6, pp.1-23, 2019.

[19] C. Moran, S. Wainerdi, T. Cherukuri, C. Kittrell, B. Wile, N. Nicholas, S. Curley, J. Kanzi and P. Cherukuri, "Size-dependent Joule heating of gold nanoparticles using capacitively coupled radio frequency," *Nano Research*, vol. 2, pp. 400-405, 2009.

[20] S. Nordebo, M. Dalarsson, Y. Ivanenko, D. Sjöberg and R. Bayford, "On the physical limitations for radio frequency absorption in gold nanoparticle suspensions," *J. Physics D: Applied Physics*, vol. 50, no. 15, 2017, Article ID 15540.

[21] C. Collins, R. McCoy, B. Ackerson, G. Collins and C. Ackerson, "Radiofrequency heating pathways for gold nanoparticles," *Nanoscale*, vol. 6, no. 15, pp. 8459–8472, 2014.

[22] N. Neshatvar, R. Damaso, N. Seifnaraghi, A. Demosthenous, and R. Bayford, "Towards a system for tracking drug delivery using frequency excited gold nanoparticles," *Sensors (Basel)*, vol. 19, no. 21, p. 4750, 2019.

[23] T. Mironava, V. Arachchilage, K. Myers and S. Suchalkin, Gold nanoparticles and radio frequency field interactions: Effects of nanoparticle size, charge, aggregation, radio frequency, and ionic background," *Langmuir*, vo. 33, no. 45, pp. 13114-13124, 2017.

[24] AdvanceEnergy, "Luxtron Fiber Optic Thermometry Probes & Accessories," Available online: https://www.advancedenergy.com.

[25] Swisstom AG, "SenTec EIT Pioneer Set," 2019. [Online] Available: http://www.swisstom.com/en/products/pioneer-set

[26] Adler, "EIDORS," [Online]. Available: http://eidors3d.sourceforge.net

[27] A. Adler, J. Arnold , R. Bayford , A. Borsic, B. Brown, P. Dixon, T. Faes, I. Frerichs , H. Gagnon, Y. Gärber , B. Grychtol , G. Hahn, W. Lionheart, A. Malik , R. Patterson , J. Stocks, A. Tizzard , N. Weiler and G. Wolf, "GREIT: a unified approach to 2D linear EIT reconstruction of lung images," *Physiol. Meas.*, vol. 30, no. 6, pp., S35-S55, 2009.

[28] Cline Scientific AB, [Online]. Available: http://www.clinescientific.com.

[29] F. Chai, C. Wang, T. Wang, L. Li and Z. Su, "Colorimetric detection of Pb2+ using glutathione functionalized gold nanoparticles," *ACS Appl. Mater. Interfaces*, vol. 2, no. 5, pp. 1466-1470, 2010.

[30] G. van Dam, G. Themelis, L. Crane, N. Harlaar, R. Pleijhuis, W. Kelder, A. Sarantopoulos, J. de Jong, H. Arts, A. van der Zee, J. Bart, P. Low, and V. Ntziachristos, "Intraoperative tumor-specific fluorescence imaging in ovarian cancer by folate receptor-α targeting: first in-human results," *Nature Medicine*, vol. 17, no. 10, pp.1315-1319, 2011.

[31] X. Liang, M. Luo, . X.-W. Wei, M. Cui-Cui, Y.-H. Yang, B. Shao, Y.-T. Liu, T. Liu, Z.-Y. He and Y.-Q. Wei, "A folate receptor-targeted lipoplex delivering interleukin-15 gene for colon cancer immunotherapy," *Oncotarget.*, vol. 7, no. 32, pp. 52207-52217, 2016.

[32] S. Jinru, D. Klimstra, J. Nitzkorskib, P. Low, M. Gonend, R. Landmann, M. Weiser, W. Franklin, F. Prendergast, L. Murphy, L. Tang, L. Temple, J. Guillem, W. D. Wong and P. Paty, "Immunohistochemical expression of folate receptor alpha in colorectal carcinoma: patterns and biological significance," *Hum. Pathol.*, vol. 39, no. 4, pp. 498-505, 2008.

[33] J. Garcia-Bermudez, R. Williams, R. Guarecuco, K. Birsoy, "Targeting extracellular nutrient dependencies of cancer cells," *Mol. Metab.*, vol. 33, p. 67-82, 2020

[34] P. S. Low and A. S. Kularatne, "Folate-targeted therapeutic and imaging agents for cancer," *Curr. Opin. Chem. Biol.*, vol. 13, no. 3, pp. 256-262, 2009.

[35] A. Cheung, H. Bax, D. Josephs, K. Ilieva, G. Pellizzari, J. Opzoomer, J. Bloomfield, M. Fittall, A. Grigoriadis, M. Figini, S. Canevari, J. Spicer, A. Tutt and S. Karagiannis, "Targeting folate receptor alpha for cancer treatment," *Oncotarget.*, vol. 7, no. 32, pp. 52553–52574, 2016.

[36] C. Martinez-Boubeta, K. Simeonidis, J. Oró, A. Makridis, D. Serantes, and L. Balcells, "Finding the limits of magnetic hyperthermia on core-shell nanoparticles fabricated by physical vapor methods," *Magnetochemistry*, vol. 7, no. 4: 49, 2021.